Geochimica et Cosmochimica Acta, 1975, Vol. 39, pp. 433 to 454. Pergamon Press. Printed in Northern Ireland

Petrography and mineral chemistry of Ca-rich inclusions in the Allende meteorite

LAWRENCE GROSSMAN
Department of the Geophysical Sciences, The University of Chicago, Chicago, Illinois 60637, U.S.A.

(*Received* 22 *May* 1974; *accepted in revised form* 7 *August* 1974)

Abstract—There are two types of white, coarse-grained, Ca–Al-rich inclusions in Allende. Type A inclusions contain 80–85 per cent melilite, 15–20 per cent spinel, 1–2 per cent perovskite and rare plagioclase, hibonite, wollastonite and grossularite. Clinopyroxene, if present, is restricted to thin rims around inclusions or cavities in their interiors. Type B inclusions contain 35–60 per cent pyroxene, 15–30 per cent spinel, 5–25 per cent plagioclase and 5–20 per cent melilite. The coarse pyroxene crystals in Type B's contain >15 per cent Al_2O_3 and >1·8 per cent Ti, some of which is trivalent. Type A pyroxenes contain <9 per cent Al_2O_3 and <0·7 per cent Ti.

Electron microprobe analyses of 600 melilite, 39 pyroxene, 35 plagioclase, 33 spinel and 20 perovskite grains were performed in 16 Type A, 1 intermediate and 9 Type B inclusions in Allende and 1 Type A in Grosnaja. Melilite composition histograms from individual Type A inclusions are usually peaked between Ak10 and Ak30 and are 15–20 mole % wide while those from Type B inclusions are broader, unpeaked and displaced to higher åkermanite contents. Most pyroxenes contain <1 per cent FeO. All plagioclase is An98 to An100. Spinel is almost pure $MgAl_2O_4$. Perovskite contains small (<1 per cent) but significant amounts of Mg, Al, Fe, Y, Zr and Nb.

Inferred bulk chemical compositions of Type A inclusions are rather close to those expected for high-temperature condensates. Those of Type B inclusions suggest slightly lower temperatures but their Ca/Al ratio seems less than the Type A's, indicating that the Type B's may not be their direct descendants. Some textural features suggest that the inclusions are primordial solid condensates while others indicate that they may have been melted after condensation. Fragmentation and metamorphism may have also occurred after condensation.

INTRODUCTION

SINCE the fall of the Allende meteorite in February, 1969, the Ca–Al-rich inclusions found in C2 and C3 chondrites have attracted considerable attention in the literature of cosmochemistry. LARIMER and ANDERS (1970) and MARVIN *et al.* (1970) were the first to suggest the unique role these objects may have played in the condensation history of the solar system, a theme which dominates the later work of GROSSMAN (1972, 1973) and GROSSMAN and CLARK (1973). Their major and trace element chemistry indicates that they may be aggregates of the highest-temperature condensates from the solar nebula. Their Sr^{87}/Sr^{86} ratios suggest that some of them are the most primitive objects yet sampled in the solar system (GRAY *et al.* 1973). The systematics of their oxygen isotopic compositions imply that they contain a component of interstellar origin which escaped homogenization at the birth of the solar system (CLAYTON *et al.* 1973).

The existence of the Ca–Al-rich inclusions is strong evidence that chemical fractionations took place during nebular condensation, an idea now common in models of planetary accretion (CLARK *et al.* 1972). In fact, several workers have concluded that the Moon is enriched in Allende inclusion-type condensates relative to chondrites (ANDERSON, 1973; WÄNKE *et al.*, 1973; KRÄHENBÜHL *et al.*, 1973).

Surprisingly little is known, however, about the petrography and mineralogy of these objects to which so much significance is attached. Several studies have appeared (e.g. CHRISTOPHE, 1968, 1969; FUCHS, 1969, 1971, 1974; CLARKE *et al.* 1970; KURAT, 1970; FROST and SYMES, 1970), but these describe a relatively small number of inclusions from a relatively large number of meteorites. This paper presents the results of a systematic petrographic and electron microprobe study of 26 coarse-grained Ca–Al-rich inclusions from the Allende carbonaceous chondrite. It is the first in a series of detailed mineralogical investigations of the different types of petrographic features in this fascinating meteorite.

PROCEDURE

Samples

Two complete Allende stones (1366 g; 1954 g) were provided by the Field Museum of Natural History for this study. Both were coated nearly continuously by fusion crust except for small areas where it was chipped. Except for one quarter of the larger stone, these samples were sliced completely into slabs using a diamond saw blade lubricated with distilled water. The slabs were from 3 to 7 mm thick. In this way a total of $\sim$2500 cm^2 of Allende were exposed to view and were examined in great detail with a stereoscopic microscope.

A bewildering array of distinct petrographic units is visible on the slab surfaces. These include various light- and dark-colored chondritic and achondritic xenoliths, from several tenths of a cm to more than 2 cm in size. Large (1–10 mm), amoeba-shaped, tan-colored olivine aggregates are common. Also present are normal olivine and pyroxene chondrules, some with thick, sulfide-bearing mantles or small cavities. Several other types of objects are present which remain unclassified pending further work.

Two types of Ca-rich inclusions are prominent. The first are commonly 1 mm–1 cm in size, are exceedingly fine-grained ($\sim$1 μm mean radius) and are ragged and elongated, sometimes appearing to be molded into shapes conformable with the surrounding chondrules. In three dimensions, some appear to be stretched into dumb-bell shapes. They exhibit a variety of colors, from white to grey to pink to purple, and often show color zonation from core to rim. On some slabs, there is a definite tendency toward the parallel alignment of the long axes of these inclusions. From published descriptions, these objects are identical to the Ca-rich 'aggregates' of CLARKE *et al.* (1970) and GRAY *et al.* (1973). These will not be discussed further here.

The second type of Ca-rich inclusion varies in size from $<$1 mm to 2 cm and is coarse-grained, often containing crystals up to 2–3 mm long. These inclusions are white and exhibit a range of shapes including subspherical, L-shaped, sinuous, pear-shaped, toroidal and crescent-shaped. Some are elongated and have rounded protuberances. They are referred to as Ca-rich 'chondrules' by CLARKE *et al.* (1970) and GRAY *et al.* (1973). It is only these coarse-grained Ca-rich inclusions which are the objects of the electron microprobe study presented here. The results of similar studies of other petrographic units in Allende will appear elsewhere.

Thirty areas of particular interest on the slabs were singled out, impregnated with an epoxy resin and made into polished thin sections having a mean diameter of $\sim$2 cm. A 34 $\times$ 27 cm photographic map was prepared for and a number given to each thin section. On every map, specific textural features were also numbered. Throughout this paper, each inclusion is identified by its thin section number, e.g. TS12, and its feature number, e.g. F3 or Feat 3.

Analytical technique

All analyses were performed with an ARL electron microprobe operated at an accelerating voltage of 15 kV and beam currents from 0·25 to 0·35 μA. The spot size was 1 μm except in the case of plagioclase analyses where it was broadened to 5 μm. The beam current was monitored and integrated to correct count rates for its variation. Drift was less than 1 per cent for all runs.

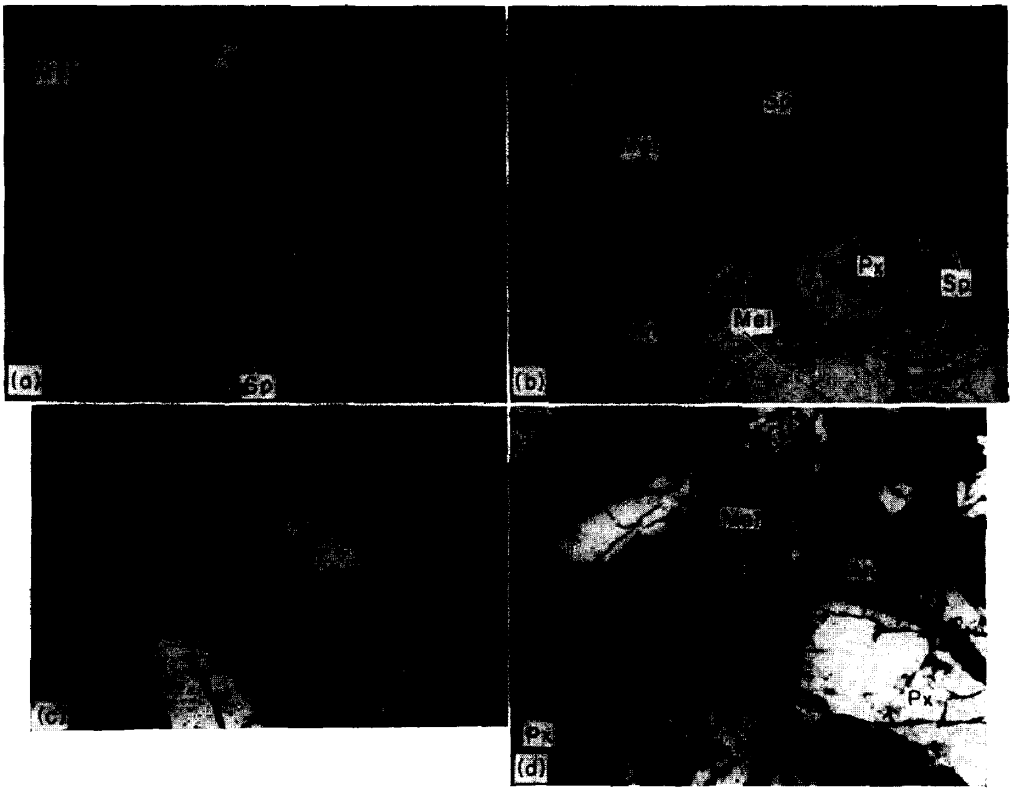

Fig. 1A. Typical Type A inclusion, TS2 F1. Light-colored phase is melilite which poikilitically encloses high-relief spinel (Sp) as single large crystals and dense concentrations of tiny grains. Thin dark lines are cleavages in the melilite. Note how fine-grained opaque material (Fg) 'spills over' the edge of the inclusion and corrodes the melilite. Mtx—Allende matrix. Width of field 2·2 mm. Plane light. B. Typical Type B inclusion, TS22 F1. Note the opaque interstitial material between the pyroxene (Px), melilite (Mel) and plagioclase (An) crystals. Note the very dense spinel (Sp) concentrations inside these phases. Width of field 2·8 mm. Plane light. C. Deformation lamellae in melilite in Type A inclusion, TS12 F1. Width of field 1·2 mm. Crossed polars. D. Typical Type B inclusion, TS23 F1, showing poikilitic spinel enclosed by anorthite (An) and melilite (Mel). Spinel is also enclosed by the pyroxene (Px) but is not visible in this photo. Note the color zonation in the melilite crystals, indicating higher åkermanite concentration in the rim than in the core. Note also the fine-grained dark interstitial material. Width of field 0·25 mm. Crossed polars.

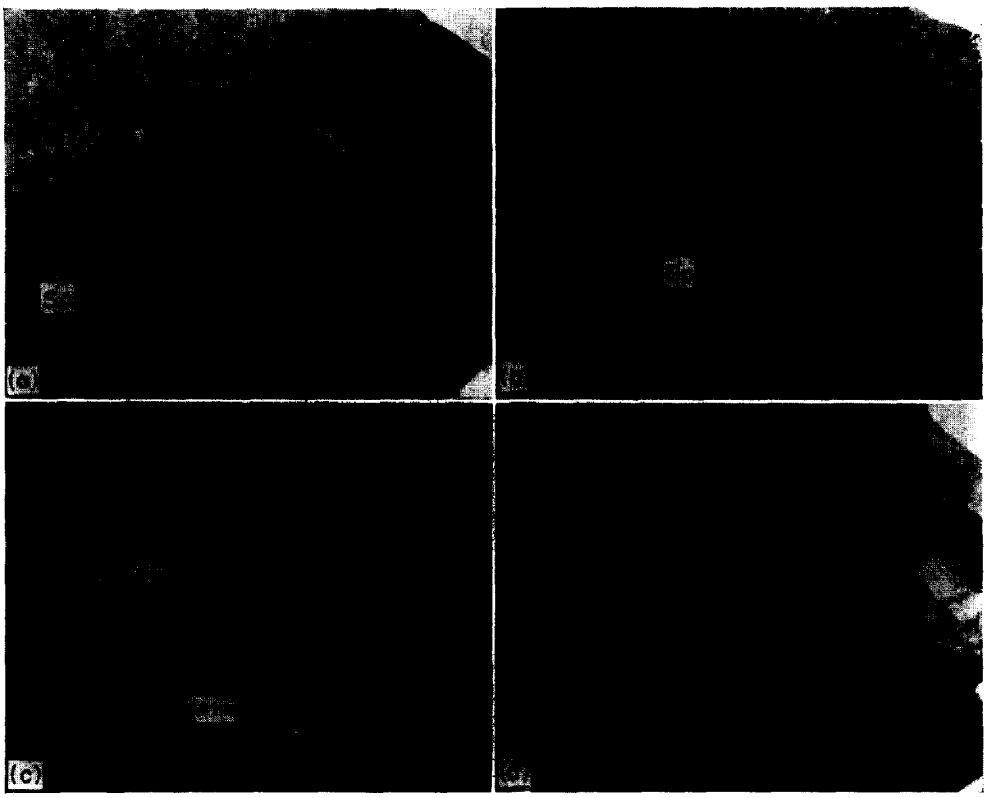

Fig. 2A. Type A inclusion, TS2 F1, showing long chains of coarse spinel crystals (Sp) and bright perovskite grains wedged between them. Host phase is melilite. Dark lines are cleavages and dark spots are pits in the section. Width of field 1 mm. Reflected light. B. Type A inclusion, TS27 F1, showing ragged, elongated spinel grains (Sp) in a matrix of recrystallized melilite. Width of field 0·3 mm. Reflected light. C. Type A inclusion, TS12 F1. Long trail of bright perovskite blebs in melilite in the outer zone of the inclusion near its contact with the matrix (Mtx). Width of field 0·92 mm. Reflected light. D. Type A inclusion, TS2 F1. Intergrowth of wormy perovskite blebs with melilite. Width of field 0·20 mm. Reflected light.

A variety of well-characterized synthetic and natural oxides and silicates were used as standards. A modified version of the computer program ABFAN2 (HADIDIACOS *et al.* 1971) was used to correct all the data for background, drift, dead-time and matrix effects. The reported concentrations of all major elements are accurate to within 2 per cent of the amounts present except where otherwise indicated. This includes errors due to counting statistics and uncertainties in the compositions of standards and in the corrections for matrix effects. Detection limits are noted on tables when count rates indicate that they are not exceeded.

PETROGRAPHY AND MINERALOGY

Types of inclusions

There are two types of coarse-grained Ca–Al-rich inclusions in Allende. Type A contains 80–85 per cent melilite, 15–20 per cent spinel and 1–2 per cent perovskite. Hibonite, plagioclase, wollastonite and grossularite are rare or absent. Clinopyroxene, if present, is restricted to thin rims around inclusions (TS24 F1) or surrounding cavities in their interiors (TS1 F1). A typical Type A inclusion is shown in Fig. 1A. Type B contains 35–60 per cent clinopyroxene, 15–30 per cent spinel, 5–25 per cent plagioclase and only 5–20 per cent melilite. Perovskite is rare in these. A typical Type B inclusion is shown in Fig. 1B. The fundamental differences between the two varieties are the abundance, morphology and composition of the clinopyroxene. This mineral is the major phase in Type B inclusions but is usually absent from Type A. When present in Type A, it makes up less than 5 per cent of the inclusion and occurs, as described above, in bands usually less than 5 μm wide. Pyroxene in Type B inclusions occurs as coarse crystals, often 1 mm in size or larger. These pyroxenes have extraordinary compositions (>15 per cent Al_2O_3 and $>1{\cdot}8$ per cent Ti) compared to those in Type A (<9 per cent Al_2O_3 and $<0{\cdot}7$ per cent Ti), although one Type B inclusion, TS18 F1, contains both varieties of pyroxene. In terms of its pyroxene compositions, one inclusion in the population studied, TS26 F1, can be regarded as intermediate between these two types (9–18 per cent Al_2O_3 and 0·9–2·4 per cent Ti). Its modal mineralogy is 30 per cent pyroxene, 50 per cent plagioclase and 20 per cent spinel. Altogether, one intermediate, 16 Type A and 9 Type B inclusions were studied from Allende and one Type A from the C3 chondrite Grosnaja.

Petrography

In thin section, a large number of Type A inclusions became visible which were not seen on slab surfaces. They are only several tenths of a mm in size and appear to be angular fragments of once larger inclusions. Although a few are almost certainly pieces of adjacent aggregates, others have no obvious spatial, textural or chemical relationships with larger inclusions in the same thin section. Because these fragments represent a significant proportion of the Type A inclusions, the mean size of the Type A's is less than that of the Type B's.

Another peculiar variety of Type A inclusion is found in Allende. It is sinuous in shape, several mm long and several tenths of a mm in width. It is purple in color and consists of tiny melilite, spinel and perovskite grains.

Melilite. This mineral is the major phase in most Type A inclusions, some of which are composed almost entirely of several 2–3 mm blocky crystals of melilite (Fig. 1A). In Type B inclusions, melilite is usually present as lath-shaped crystals

(Fig. 1D) several tenths of a mm in size. Larger blocky crystals are sometimes found in the Type B's, particularly in pyroxene-free outer zones surrounding pyroxene-rich interiors. Lamellae were observed in melilites from several inclusions of both types. These are perpendicular to the cleavage, are sometimes dagger-shaped and occur in grains with deformed cleavage planes and undulose extinction (Fig. 1C). They may have been produced by shock deformation. Several other inclusions of both types contain polycrystalline mosaics of small, interlocking melilite grains. In one case, such an area is contiguous with a remnant of a larger melilite grain which contains deformation lamellae and exhibits wavy extinction (TS27 F1). Such mosaic textures may indicate recrystallization, perhaps due to shock-induced partial melting. Reaction relations in which melilite appears to replace both plagioclase and titaniferous pyroxene (Tpx) are preserved in several Type B inclusions (e.g. TS21 F1).

Spinel. This phase almost always occurs as pink, euhedral crystals poikilitically enclosed by melilite, Tpx and plagioclase (see Figs. 1B and 1D). The spinel grains vary in size from less than 1 μm to several tenths of a mm. Host crystals contain from <5 to >70 per cent spinel by volume, with some crystals heavily laden with spinel at one end and virtually spinel-free at the other end (TS23 F1). Some melilites in Type A inclusions contain long, nearly continuous chains of euhedral spinels, often in excess of 50 crystals long (Fig. 2A). Others contain dense clouds of submicron spinels, $\sim$0·3 mm in diameter (see Fig. 1A). Anhedral spinel was found as thin rims on some Type B inclusions and as ragged, elongated grains inside areas of recrystallized melilite in one Type A inclusion (Fig. 2B). Spinel has also been reported as euhedral crystals inside Ca–Al-rich glass chondrules in Allende (MARVIN *et al.* 1970) and in Vigarano (REID *et al.* 1974).

Titaniferous pyroxene (Tpx). This is the most abundant phase in Type B inclusions, occurring in crystals up to 3 or 4 mm in size (see Figs. 1B and 1D). One inclusion with deformed melilite, TS23 F1, contains Tpx showing undulose extinction and parallel lamellae, probably due to deformation. Most Tpx is slightly pleochroic, but the most intense pleochroism is found in the most Ti-rich crystals. Grains containing 9·5–10·5 per cent Ti exhibit light greyish-green to deep bluish-green pleochroism (TS18 F1). In some inclusions Tpx appears to replace plagioclase and to be replaced by melilite.

Plagioclase. Plagioclase is very rare in Type A inclusions, but is sometimes found in association with diopside (TS24 F1). It is a common component of Type B inclusions (Fig. 1D), where it typically occurs as lath-shaped crystals surrounding and penetrating pyroxene grains. In one of these, TS21 F1, melilite and Tpx appear to be replacing plagioclase.

Diopside. This mineral is found rarely in Type A inclusions where it surrounds inclusions or cavities in their interiors. Here it forms very narrow, continuous bands of parallel crystals growing perpendicular to the edge of the inclusion and showing wavy extinction. In one instance, such a zone widens into a mosaic of polygonal grains. This inclusion, TS24 F1, is brecciated and contains deformed melilite. One Type B inclusion, TS18 F1, contains diopside texturally similar to that in Type A's, but, in contrast to it, containing up to 10 per cent FeO.

Perovskite. This phase is a common accessory in Type A inclusions. Here it can occur wedged between spinel crystals as in Fig. 2A or at spinel–melilite

interfaces. The perovskite tends to coarsen in size with its associated spinel. Rarely, wormy perovskite blebs are found intergrown with melilite (Fig. 2D). A continuous zone of rounded perovskite blebs often surrounds entire inclusions of either type just inside their contacts with the matrix (see Fig. 2C). In Type B inclusions, this is typically the only mode of occurrence of perovskite.

Other phases. Hibonite was discovered on the edge of one Type A inclusion, TS12 F1, where a reddish luminescence under the electron beam signalled its presence. White acicular crystals were observed on slab surfaces in cavities of both types of inclusions. This mineral is tentatively identified as wollastonite on the basis of its morphology. Grossularite lines were found in X-ray diffraction patterns of some inclusions of both types. This mineral was searched for but never found in thin section. It must be a very minor phase in these inclusions or else it is heterogeneously distributed. Olivine occasionally forms discontinuous, fine-grained monomineralic crusts on the surfaces of both types of inclusions (e.g. TS25 F1). Twenty-one olivine analyses from three inclusions showed a range in composition from Fo65 to Fo95 and a mean of Fo81. Nickel–iron grains up to several microns in size occur rarely inside some Type A and Type B inclusions. These are in the form of rounded to angular grains surrounded by silicates or rounded blebs inside perovskite grains (TS19 F1). Often they are associated with fractures which stretch out to the matrix but sometimes no fractures are present.

Edge effects. On slab surfaces, it can be seen that the matrix darkens in color in a narrow zone immediately adjacent to most of the objects comprising the coarse-grained fraction of Allende. As mentioned above, some of the Ca-rich inclusions also possess olivine overgrowths attached to their outer edges. In addition, thin section examination reveals that almost every inclusion of both types contains a region of very fine-grained, opaque, greyish-brown to reddish-brown material just to the inside of its contact with the matrix (Fig. 1A). This material forms irregular patches which appear to be replacing the primary silicate minerals discussed above, particularly plagioclase and melilite. Sometimes these regions continue along fractures or grain boundaries deep into the interiors of the inclusions where alteration of the silicates takes place and the textural relations between the primary minerals are obscured (see Figs. 1B and 1D). Some inclusions contain up to 65 % of this material.

Mineral chemistry

Melilite. This phase was always found to contain less than several tenths of a per cent Na_2O and FeO, only achieving these levels when closely associated with fine-grained alteration material. The uncertainties in the concentrations of these elements are ± 20 per cent of the amount present at the 0·07 per cent Na_2O level and ± 34 per cent on 0·11 per cent FeO, largely due to poor counting statistics. Table 1 shows some representative analyses. Similar melilite compositions were reported by CLARKE *et al.* (1970), KURAT (1970), FUCHS (1971, 1974), MALISSA *et al.* (1972), REID *et al.* (1974) and GRAY *et al.* (1973). Unlike most terrestrial melilites which contain appreciable Na_2O, the melilite in these inclusions can be considered as a two-component solid solution between gehlenite ($Ca_2Al_2SiO_7$) and åkermanite ($Ca_2MgSi_2O_7$). Ca, Al, Mg and Si concentrations were determined

Table 1. Analyses of melilites in Allende inclusions

	TS7 F3 9	TS12 F1 128	TS12 F3* 186	TS12 F1 116	TS2 F1 57	TS2 F1 30	TS2 F1 65
Na_2O	<0·02	0·04	<0·02	<0·02	<0·02	0·09	0·07
Al_2O_3	34·27	30·72	29·12	27·32	21·05	17·50	15·25
MgO	1·26	2·47	2·84	3·63	6·30	7·77	8·51
TiO_2	<0·04	<0·04	<0·04	<0·04	<0·04	<0·04	<0·04
FeO	<0·05	<0·05	0·11	<0·05	<0·05	<0·05	<0·05
SiO_2	24·18	25·36	26·31	27·20	30·84	33·12	35·36
CaO	40·66	41·06	41·18	41·50	41·53	41·54	40·75
Sum	100·37	99·65	99·56	99·65	99·72	100·02	99·94
Mole % Ak							
Al	8·45	17·0	21·3	26·1	43·2	52·9	59·2
Mg	8·49	16·9	19·4	24·9	43·1	52·9	57·6
Si	9·55	16·2	20·7	24·7	41·3	51·1	60·6

* Melilite from a Type B inclusion.

in randomly selected spots in melilite. These analyses were performed in 548 points in the Allende inclusions and in 49 points in a single inclusion in Grosnaja. The mole per cent åkermanite in a melilite can be calculated from either the Al, the Mg or the Si content. As seen in Table 1, the åkermanite contents derived from the concentrations of different elements in one spot often differed by as much as 2–3 mole %. Errors due to counting statistics for Mg exceed ± 1 per cent below 37 mole % åkermanite (Ak37), rising to ± 8 per cent at Ak5. Similarly, counting uncertainty for Al exceeds ± 1 per cent at Ak40 and becomes poorer at higher åkermanite contents. In sharp contrast, the precision of the Si determinations is always better than $\pm 0{\cdot}6$ per cent. Because of this and the fact that Si has the highest atomic number of the three elements and requires the smallest relative corrections due to matrix effects, all åkermanite contents reported here are based on the Si analyses.

Åkermanite contents commonly vary by 5–10 mole % from place to place within a crystal. In one extreme case in a Type A inclusion, TS2 F1, the melilite composition within a single large crystal varies continuously from Ak29 in some areas to Ak65 in others, with the interference colors changing from first order grey or anomalous blue to a deep orange in areas exceeding Ak50. These high åkermanite patches are rounded and irregular and bear no consistent spatial relationship to the rest of the crystal. Some patches are found at one end of the crystal, another to one side and still another near the center. Pronounced concentric zoning of melilite crystals is rare. One Type B inclusion, TS23 F1, was found to contain melilite whose rim is richer in åkermanite than its core. This zoning is evident in Fig. 1D.

Histograms of melilite compositions in several representative Type A inclusions are shown in Fig. 3. These histograms usually peak between Ak10 and Ak30 and are 15–20 mole % wide. The exceptions are TS27 F1 whose melilite is very low in åkermanite and TS2 F1 which is very high and variable. The Grosnaja inclusion seems to fit nicely into this group. Owing to the small size of a number

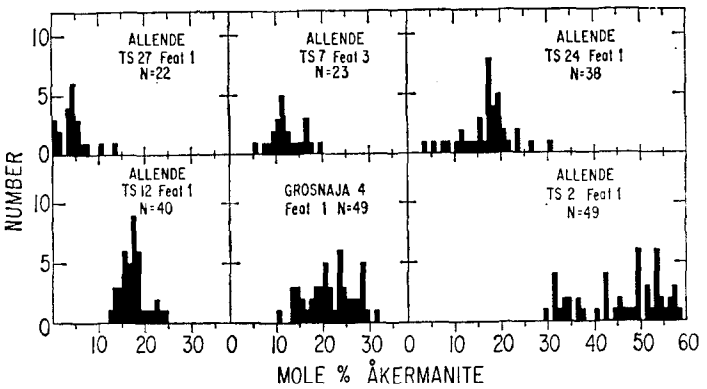

Fig. 3. Melilite composition histograms for individual Type A inclusions. These are usually peaked between Ak10 and Ak30 and are 15–20 mole % wide. The Grosnaja inclusion is very similar to the Type A inclusions in Allende. TS2 F1 is higher in åkermanite and broader than the others.

of the Type A inclusions, fewer than 15 melilite analyses each are available for several of them.

Figure 4 shows histograms of 6 representative Type B inclusions. In contrast to the Type A's, these tend to be relatively broad and unpeaked. They are commonly more than 25 mole % wide and tend to show mean values above Ak35. The exception is TS12 F3 whose histogram resembles that of a Type A inclusion.

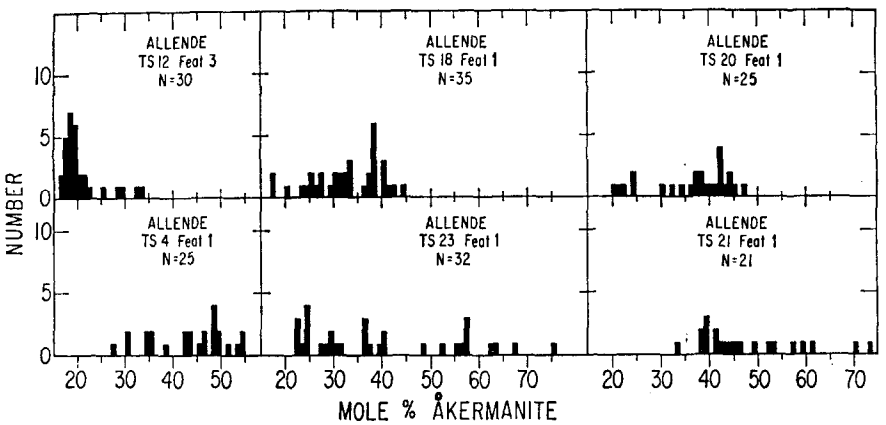

Fig. 4. Melilite composition histograms for individual Type B inclusions. These are relatively broad and unpeaked compared to those in Fig. 3. They are, on the average, higher in åkermanite than the Type A's.

The melilite compositions from all Type A and all Type B Allende inclusions are plotted on separate histograms and compared to each other in Fig. 5. As a group, the Type A inclusions stretch from Ak0 to Ak58, peak at Ak15–Ak20 and show a high åkermanite tail. The Type B inclusions range between Ak15 and Ak75 and exhibit a relatively flat distribution between Ak15 and Ak50 with a high åkermanite tail. Although there is considerable overlap between the two

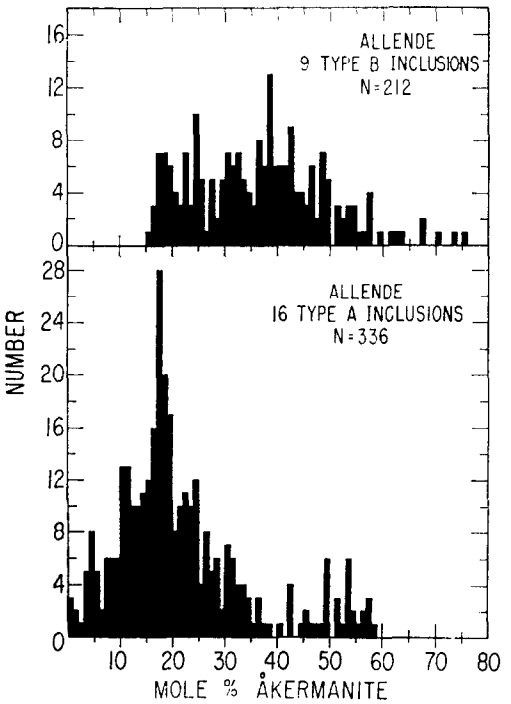

Fig. 5. All Type A melilite analyses compared to all Type B data for Allende. The Type A melilites peak in frequency between Ak15 and Ak20. The Type B melilites show a relatively flat distribution between Ak15 and Ak50. Melilite from Type B inclusions has a higher åkermanite content, on the average, than that in Type A inclusions. Both frequency distributions show a high åkermanite tail.

histograms, there is an apparent trend toward higher åkermanite contents in the melilites of Type B inclusions.

Pyroxene. A total of 115 points were analyzed in 5 pyroxene grains in 2 Type A inclusions and 34 grains in 10 Type B inclusions. Their Al_2O_3 and TiO_2 contents are plotted in Fig. 6. Table 2 shows the range of pyroxene compositions found in Type A inclusions. Because of the lower precision due to counting statistics, the accuracy of the TiO_2, Al_2O_3 and FeO analyses becomes poorer than ± 2 per cent of the amounts present when their concentrations fall below 10 per cent. These errors increase to ± 4 per cent at 1·50 per cent TiO_2, ± 7 per cent at 0·6 per cent Al_2O_3 and ± 27 per cent at 0·09 per cent FeO.

In Fig. 6 and every table of pyroxene analyses, all Ti is calculated as Ti^{4+}. The numbers of cations are calculated on the basis of 6 oxygen atoms. The assignment of Al to tetrahedral and octahedral sites is based on the assumption that Si and Al are the only two tetrahedral cations and that there must be 2·00 such cations for every 6 oxygen atoms. All of the Type A pyroxenes contain very little iron which is assumed to be divalent as would be the case under high temperature solar nebular reducing conditions. They range in composition from nearly pure diopside to pyroxenes containing up to 8·99 per cent Al_2O_3 and are similar

Table 2. Analyses of pyroxenes in Type A Allende inclusions

	TS24 F1 2B	TS24 F1 4B	TS24 F1 3C	TS1 F1 3A	TS24 F1 4C
MgO	19·01	18·21	16·43	16·39	15·29
Al_2O_3	0·71	2·07	3·05	6·57	8·99
SiO_2	55·01	53·51	55·32	51·59	49·75
CaO	26·80	27·27	25·16	26·25	26·50
TiO_2*	<0·03	<0·03	<0·03	0·65	1·15
FeO	<0·03	0·07	0·13	0·32	0·08
Sum	101·53	101·13	100·09	101·77	101·76
	Numbers of cations on the basis of 6(0)				
Si	1·96	1·92	1·98	1·84	1·77
Al	0·03	0·08	0·02	0·16	0·23
Sum	1·99	2·00	2·00	2·00	2·00
Al	0·00	0·01	0·11	0·12	0·15
Ti	0·00	0·00	0·00	0·02	0·03
Mg	1·01	0·97	0·88	0·87	0·81
Fe	0·00	0·00	0·00	0·01	0·00
Ca	1·02	1·05	0·97	1·00	1·01
Sum	2·03	2·03	1·96	2·02	2·00

* All Ti calculated as Ti^{4+}.

Table 3. Analyses of pyroxenes from Type B inclusions, showing the range of Al_2O_3 contents and average TiO_2 contents

	TS23 F1 4A	TS4 F1 2A	TS21 F1 4A	TS8 F3 1C	TS4 F1 4A	TS21 F1 2A	TS8 F3 2B
MgO	11·51	10·23	10·48	10·36	9·34	8·96	8·09
Al_2O_3	15·14	15·94	16·74	17·89	19·15	19·91	21·38
SiO_2	42·90	40·55	41·32	40·32	38·57	38·53	35·73
CaO	26·02	25·02	25·94	26·22	25·11	25·47	25·64
TiO_2*	6·01	7·58	6·97	6·79	7·58	7·76	7·41
FeO	<0·03	0·49	0·04	0·27	0·57	0·36	<0·03
Sum	101·58	99·81	101·49	101·85	100·32	100·99	98·25
	Numbers of cations on the basis of 6(0)						
Si	1·54	1·49	1·49	1·46	1·41	1·40	1·34
Al	0·46	0·51	0·51	0·54	0·59	0·60	0·66
Sum	2·00	2·00	2·00	2·00	2·00	2·00	2·00
Al	0·18	0·18	0·20	0·22	0·24	0·25	0·28
Ti	0·16	0·21	0·19	0·18	0·21	0·21	0·21
Mg	0·62	0·56	0·56	0·56	0·51	0·49	0·45
Fe	0·00	0·02	0·00	0·01	0·02	0·01	0·00
Ca	1·00	0·99	1·00	1·01	0·99	0·99	1·03
Sum	1·96	1·96	1·95	1·98	1·97	1·95	1·97

* All Ti calculated as Ti^{4+}.

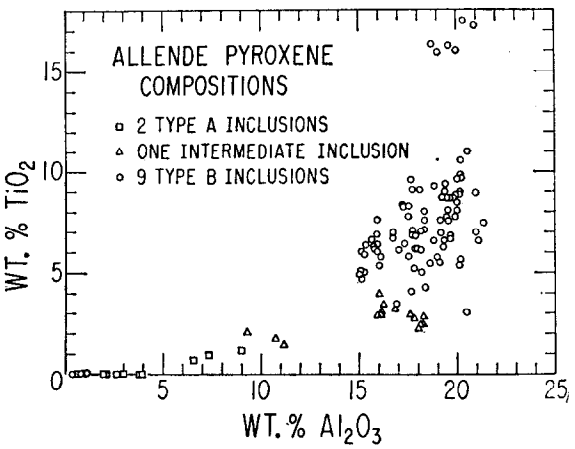

Fig. 6. Pyroxenes in Type B inclusions contain extraordinarily high Al_2O_3 and Ti concentrations. Pyroxenes in Type A inclusions are close to pure diopside, containing less Al_2O_3 and Ti than those in Type B. All Ti is calculated as TiO_2 but a large fraction of the Ti must be trivalent.

to those described by KURAT (1970) and REID *et al.* (1974). With increasing Al_2O_3 content, the numbers of tetrahedral and octahedral Al ions both increase as Mg and Si decrease. Type A pyroxenes are generally poor in Ti, although the highest-Al_2O_3 pyroxenes contain larger amounts, up to 1·15 per cent TiO_2.

In Table 3, some analyses of Type B pyroxenes of rather typical TiO_2 content are listed in order of increasing Al_2O_3 content. The Al_2O_3 concentration was found to range from 15·14 to 21·38 per cent and the most common TiO_2 content is between 6 and 8 per cent. These pyroxenes are thus far more Al- and Ti-rich than those found in Type A inclusions and are similar to those reported by FROST and SYMES (1970) and CLARKE *et al.* (1970). FeO is always less than 1 per cent. In addition to the data in Table 3, Cr_2O_3 was determined in 9 Type B pyroxenes. They were found to have very low Cr_2O_3 contents, between 0·07 and 0·14 per cent, corresponding to a range of 0·002–0·004 Cr cations per 6 oxygen atoms.

In the type B pyroxenes, as the Al_2O_3 content increases, the numbers of tetrahedral Si and octahedral Mg cations again both decrease. In contrast to the Type A inclusions, the number of octahedral cations in these pyroxenes is consistently slightly below 2·00. This is also apparent in Table 4, where Type B pyroxenes of average Al_2O_3 content are listed in order of increasing TiO_2 concentration. The consistently low cation sums suggest that a poor choice of valence has been made for one of the metals, but Ti is the only metal present in significant quantities which exhibits variable valence. As the TiO_2 content increases from 3·06 to 17·49 per cent in Table 4, the number of octahedral cations decreases from 1·98 to 1·88. Furthermore, the pyroxenes having the highest Ti content in Table 4 are the ones with the most intense pleochroism which may indicate a charge transfer reaction. The available evidence thus suggests that Ti is present in the +3 and +4 valence states in the Type B pyroxenes. DOWTY and CLARK (1973) argued for the existence of Ti^{3+} in a pyroxene from a Type B inclusion in Allende based on its chemical, structural and spectral properties. At least $\frac{1}{3}$, but usually $\frac{2}{3}$,

Table 4. Analyses of pyroxenes from Type B inclusions, showing the range of TiO_2 contents and average Al_2O_3 contents

	TS12 F3 8	TS8 F3 3C	TS23 F1 5B	TS12 F3 20	TS4 F1 4C	TS4 F1 1C	TS12 F3 21	TS18 F1 2B	TS18 F1 2A
MgO	9·71	10·35	10·52	9·44	9·90	8·62	8·07	7·20	6·81
Al_2O_3	20·46	18·38	18·21	18·16	18·20	19·58	19·46	19·93	20·35
SiO_2	40·61	41·41	41·97	39·60	39·31	37·08	37·17	32·77	31·98
CaO	25·82	25·72	25·93	24·94	25·03	25·38	24·77	24·68	24·63
TiO_2*	3·06	4·28	5·01	6·08	7·02	8·07	9·35	16·00	17·49
FeO	<0·03	0·13	<0·03	<0·03	0·49	<0·03	<0·03	<0·03	<0·03
Sum	99·66	100·27	101·64	98·22	99·95	98·73	98·82	100·58	101·26
	Numbers of cations on the basis of 6(0)								
Si	1·48	1·51	1·51	1·47	1·44	1·38	1·38	1·21	1·18
Al	0·52	0·49	0·49	0·53	0·56	0·62	0·62	0·79	0·82
Sum	2·00	2·00	2·00	2·00	2·00	2·00	2·00	2·00	2·00
Al	0·36	0·30	0·28	0·27	0·23	0·24	0·23	0·08	0·06
Ti	0·08	0·12	0·14	0·17	0·19	0·23	0·26	0·45	0·48
Mg	0·53	0·56	0·56	0·52	0·54	0·48	0·45	0·40	0·37
Fe	0·00	0·00	0·00	0·00	0·02	0·00	0·00	0·00	0·00
Ca	1·01	1·00	1·00	0·99	0·99	1·01	0·99	0·98	0·97
Sum	1·98	1·98	1·98	1·95	1·97	1·96	1·93	1·91	1·88

* All Ti calculated as Ti^{4+}.

of the Ti must be calculated as Ti_2O_3 in order to bring the sum of the octahedral cations to 2·00 in the high-Ti pyroxenes studied here. The two pyroxenes with the highest Ti contents in Table 4 have slightly higher Al_2O_3 contents than the others, yet the number of octahedral Al ions is considerably less. Correspondingly, the number of tetrahedral Al and octahedral Ti ions is higher in these than in the remaining pyroxenes. If the same number of tetrahedral and octahedral Al ions are assigned as in the others, then approximately $\frac{1}{3}$ of the Ti ions are required to fill the vacated tetrahedral sites. This is the same as our estimate, above, of the fraction of the Ti ions which are quadrivalent. This may mean that Ti^{4+} and Al^{3+} are substituting for Si^{4+} in tetrahedral sites while Mg^{2+}, Al^{3+} and Ti^{3+} are present in octahedral sites. Pyroxenes of constant Al_2O_3 content exhibit a negative correlation between their Ti and both their Mg and Si concentrations. Fuchs (1971) and Gray *et al.* (1973) described pyroxenes similar in composition to those in Table 4.

The variation in composition within a pyroxene crystal is often large compared to the difference in composition observed between grains in the same Type B inclusion. One crystal in TS12 F3 was studied in detail. Its rim contains 3·06 per cent TiO_2, 20·46 per cent Al_2O_3, 9·71 per cent MgO and 40·61 per cent SiO_2 and its core contains 7·74 per cent TiO_2, 19·50 per cent Al_2O_3, 8·66 per cent MgO and 39·76 per cent SiO_2. A region between these two, but closer to the rim, contains 8·95 per cent TiO_2, 20·98 per cent Al_2O_3, 7·59 per cent MgO and 38·55 per cent SiO_2. Several pyroxene crystals were seen which had strongly pleochroic cores and non-pleochroic rims.

Table 5 shows some infrequently encountered pyroxene compositions. The first two are from the same Type B inclusion, TS18 F1, which contains the very Ti-rich, pleochroic pyroxenes. They occur in fine-grained crusts with olivine on

Table 5. Infrequently encountered pyroxene compositions from one Type B and one intermediate inclusion

	TS18 F1† 3A	TS18 F1† 3C	TS26 F1 1B	TS26 F1 2B	TS26 F1 4A	TS26 F1 5C	TS26 F1 3B
MgO	17·99	14·40	15·22	14·62	11·89	11·83	11·40
Al_2O_3	0·81	0·39	9·28	11·11	16·03	16·82	18·02
SiO_2	56·43	47·55	47·96	47·80	42·78	43·75	43·05
CaO	24·83	25·84	25·67	25·93	25·18	25·07	25·98
TiO_2*	<0·03	<0·03	2·08	1·45	3·95	3·20	2·25
FeO	0·09	10·36	0·16	0·27	0·17	0·21	0·43
Sum	100·15	98·54	100·37	101·18	100·00	100·88	101·13
	Numbers of cations on the basis of 6(0)						
Si	2·02	1·86	1·74	1·72	1·56	1·57	1·55
Al	0·00	0·02	0·26	0·28	0·44	0·43	0·45
Sum	2·02	1·88	2·00	2·00	2·00	2·00	2·00
Al	0·03	0·00	0·14	0·19	0·25	0·28	0·32
Ti	0·00	0·00	0·06	0·04	0·11	0·09	0·06
Mg	0·96	0·84	0·82	0·78	0·65	0·63	0·61
Fe	0·00	0·34	0·00	0·01	0·01	0·01	0·01
Ca	0·95	1·08	1·00	1·00	0·98	0·97	1·00
Sum	1·94	2·26	2·02	2·02	2·00	1·98	2·00

* All Ti calculated as Ti^{4+}.

† Pyroxene from a Type B inclusion.

the outer edges of this inclusion and are similar in composition to Type A pyroxenes, except for the high FeO. The remaining analyses in Table 5 are of pyroxenes from a melilite-free, plagioclase-rich inclusion. They are intermediate in Al and Ti between Type A and Type B inclusions. MARVIN *et al.* (1970) and MALISSA *et al.* (1972) reported the occurrence of Ti-poor, Fe–Al-rich pyroxenes in Allende, and FUCHS (1969) described an Fe-poor, Ti–Al-rich orthopyroxene.

Plagioclase. Over 100 points were analyzed in 35 plagioclase grains in 7 Type B inclusions. Seventy-five per cent of the analyses fall between An99 and

Table 6. Spinel analyses from Type A and Type B inclusions

	TS27 F1 X–A	TS25 F1 Y–D	TS23 F1 X–B*	TS24 F1 X–B	TS23 F1 Y–C†	TS2 F1 X–B–E	TS2 F1 X–A–D	TS25 F1 X–D	TS12 F3 Y–B†	TS12 F1 X–D
MgO	27·90	25·09	28·20	27·78	28·25	28·05	28·08	26·77	27·95	28·04
Al_2O_3	71·10	69·13	70·94	69·94	70·74	70·49	70·91	68·99	69·49	69·86
CaO	0·51	0·28	0·28	0·34	0·13	0·13	0·14	1·00	0·27	0·14
TiO_2	0·12	0·13	0·25	0·25	0·35	0·56	0·58	0·66	0·76	1·51
Cr_2O_3	<0·01	0·11	0·20	0·13	0·18	0·25	0·20	0·13	0·58	0·17
FeO	0·06	4·67	0·43	0·17	0·11	0·49	<0·02	1·87	<0·02	0·05
Y_2O_3	0·04	0·04	<0·01	<0·01	<0·01	<0·01	<0·01	<0·01	<0·01	0·02
ZrO_2	<0·02	<0·02	<0·02	<0·02	0·04	<0·02	<0·02	<0·02	<0·02	<0·02
Nb_2O_5	0·04	<0·03	<0·03	<0·03	<0·03	<0·03	<0·03	<0·03	<0·03	<0·03
Sum	99·77	99·45	100·30	98·61	99·80	99·97	99·91	99·42	99·05	99·79

* Spinel enclosed by melilite in a Type B inclusion.

† Spinel enclosed by pyroxene in a Type B inclusion.

All other spinels are enclosed by melilite in Type A inclusions.

An100 with the remainder between An98 and An99, consistent with the data of CLARKE *et al.* (1970) for plagioclase in a Type B inclusion. K_2O is usually below detectability (<0·01 wt. %), but some analyses show K_2O contents as high as 0·05 per cent.

Spinel. Thirty-three spinels were analyzed in 5 Type A and 2 Type B inclusions. All Ti is assumed to be Ti^{4+}. The Cr_2O_3 and TiO_2 contents of all spinels analyzed are plotted in Fig. 7. Similarly, their FeO and CaO concentrations are shown in Fig. 8. Some representative analyses are given in Table 6. The reported concentrations are accurate to within ±8 per cent of the amount present at a level of 0·28 per cent CaO, ±8 per cent at 0·35 per cent TiO_2, ±11 per cent at 0·20 per cent Cr_2O_3, ±7 per cent at 0·49 per cent FeO, ±70 per cent at 0·04 per cent Y_2O_3, ±75 per cent at 0·04 per cent ZrO_2 and ±100 per cent at 0·04 per cent Nb_2O_5. The remarkable feature of the spinels is how close they are in composition to pure $MgAl_2O_4$. All Cr_2O_3 and most FeO, CaO and TiO_2 contents are well below 1 per cent. Several Type A spinels contain more than 1·5 per cent TiO_2 or CaO and others contain 1–5 per cent FeO. The analyses shown in Table 6 are quite similar to those of spinels in Ca-rich inclusions reported by CHRISTOPHE

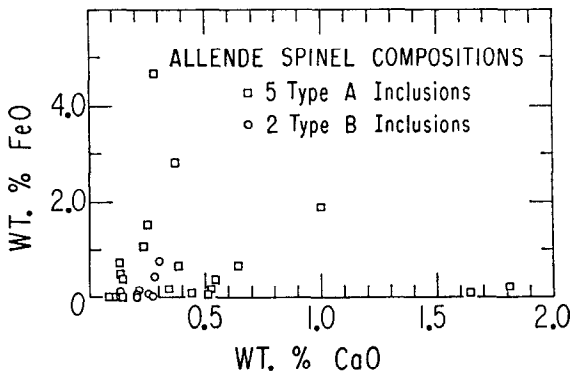

Fig. 7. FeO and CaO contents of spinels. The spinels in these inclusions are remarkably close in composition to pure $MgAl_2O_4$, although CaO and FeO concentrations sometimes exceed one per cent.

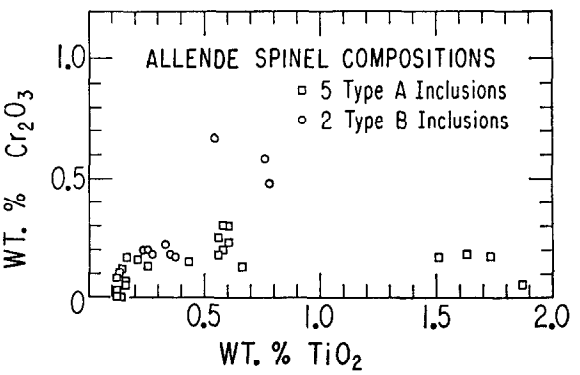

Fig. 8. Cr_2O_3 and TiO_2 contents of spinels in Allende inclusions seldom exceed 1 per cent.

Table 7. Perovskite and hibonite analyses from Type A inclusions

	TS2 F1 X–B–D	TS2 F1 X–A–C	TS24 F1 Y–C	TS24 F1 X–C	TS12 F1 X–B	TS12 F1 X–C	TS25 F1 X–C	TS12 F1 X–G*
MgO	0·15	0·13	0·08	0·06	0·13	0·13	0·23	0·53
Al_2O_3	0·31	0·28	0·68	0·39	0·28	0·24	1·45	86·58
CaO	40·97	41·41	40·79	41·02	40·32	40·63	40·21	8·13
TiO_2	57·07	57·17	56·97	56·16	57·38	57·52	54·85	1·59
Cr_2O_3	<0·01	<0·01	<0·01	0·03	<0·01	<0·01	0·02	0·05
FeO	0·03	<0·02	<0·02	<0·02	0·15	0·18	0·07	0·60
Y_2O_3	<0·02	<0·02	0·10	0·03	0·21	0·12	0·09	<0·02
ZrO_2	0·09	0·08	0·12	0·17	0·30	0·47	0·68	0·07
Nb_2O_5	<0·04	0·29	<0·04	<0·04	<0·04	<0·04	<0·04	<0·04
Sum	98·62	99·36	98·74	97·86	98·77	99·29	97·60	97·55

* Hibonite.

(1968), FUCHS (1969, 1971), FROST and SYMES (1970), REID *et al.* (1974) and GRAY *et al.* (1973). Some spinels richer in FeO have been described by KURAT (1970), MARVIN *et al.* (1970) and MALISSA *et al.* (1972). Relatively few spinels were analyzed in Type B inclusions and any suggestion of compositional differences between these and Type A spinels may simply be due to the small number of analyses. Similarly, no systematic differences are evident between spinels enclosed by melilite and those surrounded by pyroxene in Type B inclusions, although little data of this type were collected.

Perovskite. Twenty perovskite grains were analyzed in 4 Type A inclusions. Some representative compositions are shown in Table 7. The perovskite in these inclusions is virtually pure $CaTiO_3$ with minor amounts (usually <1 per cent) of MgO, Al_2O_3, Cr_2O_3 and FeO. Uncertainties in concentrations are ± 12 per cent of the amount present at 0·13 per cent MgO, ± 12 per cent at 0·28 per cent Al_2O_3, ± 60 per cent at 0·03 per cent Cr_2O_3 and ± 19 per cent at 0·15 per cent FeO. These perovskites are similar in composition to those in Type A (KURAT, 1970) and Type B (FROST and SYMES, 1970) inclusions in Lancé. There are also small, but significant, quantities of Y_2O_3, ZrO_2 and, sometimes, Nb_2O_5 in solid solution. Errors due to counting statistics are ± 20 per cent on 0·12 per cent Y_2O_3, ± 10 per cent on 0·30 per cent ZrO_2 and ± 20 per cent on 0·29 per cent Nb_2O_5. The concentrations of Y_2O_3 and ZrO_2 shown in Table 7 are considerably lower than those reported by KURAT (1970) in perovskite from a Type A Ca–Al-rich inclusion in Lancé.

Hibonite. A single analysis is reported in the final column of Table 7. It is very similar to analyses of the reddish-orange luminescent variety of hibonite reported by KEIL and FUCHS (1971) from Type A Ca–Al-rich inclusions in Leoville and Allende and corresponds to the formula

$$Ca_{0.999}O \cdot 6[(Al_{1.951}Ti_{0.023}Mg_{0.015}Fe_{0.010})O_3].$$

Fine-grained material. Two regions were studied in the opaque border zone of TS2 F1, a Type A inclusion (Fig. 1A). The compositions of 5 spots are shown in Table 8. These areas are rich in CaO and Al_2O_3 but are sometimes higher in Na_2O and FeO than the melilite and spinel which constitute the interior of the inclusion. The large variation in composition from spot to spot implies the presence of more than one phase but the analyses indicate that these regions are not simply fine-grained mixtures of melilite and spinel. Probably because of the small grain size

Table 8. Analyses of fine-grained opaque material

	TS2 F1 A-12	TS2 F1 A-16	TS2 F1 A-13	TS2 F1 B-3	TS2 F1 B-4
Na_2O	0·16	0·49	0·29	0·03	0·09
Al_2O_3	30·41	36·89	30·28	3·33	22·95
MgO	1·95	2·56	1·56	23·94	6·55
TiO_2	<0·04	<0·04	<0·04	<0·04	<0·04
FeO	0·80	1·60	1·79	<0·05	0·25
SiO_2	35·69	36·68	44·92	39·58	37·47
CaO	30·36	24·45	23·55	35·99	34·39
Total	99·37	102·67	102·39	102·87	101·70

and heterogeneous nature of this material, considerable difficulty was encountered in analyzing it, and many other attempts resulted in sums of oxide concentrations which were far from 100 per cent. Some of these gave Na_2O contents greater than 1 per cent.

Discussion

Bulk chemical compositions of inclusions

Knowing the mean compositions of the component phases, it is possible to compute the bulk chemical compositions of the inclusions if the relative abundances of the phases can be ascertained. In performing this calculation, rare phases such as hibonite and grossularite are neglected. Similarly, the fine-grained, opaque interstitial alteration material is ignored, leaving a composition which represents only the primary mineralogy of the inclusions.

Determining the modal analysis is relatively easy for Type A inclusions because they have a simple mineralogy dominated by only two phases, melilite and spinel. Chemical compositions were calculated for extremes of observed spinel/melilite ratios. The composition of the average Type A inclusion must lie between these two extremes, listed in Table 9.

Estimating the volume percentages of the various minerals in Type B inclusions

Table 9. Calculated compositions of Type A and Type B inclusions compared to calculated condensate compositions at $P_{tot} = 10^{-3}$ atm

	Condensate 1500°K	Mean Type A inclusion (i)	Mean Type A inclusion (ii)	Condensate 1475°K	Mean Type B inclusion (iii)	Mean Type B inclusion (iv)	Mean Type B inclusion (v)	Mean Type B inclusion (vi)	Coarse-grained inclusion*	Condensate 1450°K	Condensate 1440°K
CaO	35·70	29·71	36·49	32·31	17·69	18·09	21·45	20·75	26·76	27·23	18·86
Al_2O_3	38·78	41·75	35·07	34·81	40·27	37·30	32·81	31·72	31·61	29·22	20·21
TiO_2	1·95	0·84	0·79	1·77	2·99	3·68	3·73	4·39	0·99	1·49	1·02
MgO	4·25	9·72	5·43	9·39	15·37	14·55	12·03	12·59	10·82	16·98	21·03
SiO_2	19·32	17·99	22·20	21·71	23·68	26·36	30·01	30·55	29·79	25·09	38·87
Total	100·00	100·01	99·98	99·99	100·00	99·98	100·03	100·00	99·97	100·01	99·99
				Estimated modal mineralogy							
Melilite		74	89		15	10	15	10			
Spinel		25	10		35	30	20	20			
Perovskite		1	1		0	0	0	0			
Pyroxene		0	0		40	50	50	60			
Anorthite		0	0		10	10	15	10			
Total		100	100		100	100	100	100			

* Clarke *et al.* (1970) Type A chondrule NMNH 3529.

is somewhat more difficult, primarily because of the larger number of phases and because of the heterogeneous distribution of spinel within individual inclusions and even within individual host mineral grains. The calculations are performed over observed ranges of mineralogical compositions which bracket the average modal analysis determined for Type B inclusions. The concentration of any oxide in the average Type B inclusion lies between the extremes listed in Table 9.

It is evident that the average Type A inclusion is considerably richer in CaO and probably Al_2O_3 than the average Type B inclusion. The Type A's appear to be poorer in TiO_2, MgO and SiO_2 than the Type B's. Two calculated Type B composition limits (v) and (vi), are similar to the bulk chemical analysis of the coarse-grained inclusion reported by CLARKE *et al.* (1970) which, from its mineralogy, would be a Type B inclusion according to the classification scheme adopted in this paper. As seen in the table, however, its CaO content is considerably higher and its SiO_2, Al_2O_3 and MgO contents slightly lower than the estimated compositions. This may signify a higher content of anorthite and melilite and lower spinel than the limits computed here.

Also shown in Table 9 are calculated bulk compositions of the solar nebula condensate assemblage (excluding nickel–iron) at several temperatures at 10^{-3} atm total pressure, as calculated by GROSSMAN (1972) and updated in GROSSMAN (1974). The average Type A inclusion has a composition rather close to that expected for the equilibrium condensate assemblage between 1475° and 1500°K. The TiO_2 content of the inclusions is relatively low, but this could be due to an underestimate of the perovskite content, a minor phase which is heterogeneously distributed. In addition, the range of åkermanite contents of the melilites in Type A inclusions suggests nebular equilibration temperatures in the area of 1475–1500°K (GROSSMAN, 1974). Also, the diopside rims surrounding some Type A's indicate that the minerals in their interiors condensed above 1442°K. The mean Al_2O_3 and MgO contents of the Type B's, however, suggest condensation temperatures between 1450° and 1475°K and their mean CaO and SiO_2 contents indicate temperatures between 1440° and 1450°K. It is unlikely that this apparent temperature discordance is due to poor estimates of the modal mineralogy since, in that case, even the limits to the mean composition of the Type B inclusions would have to contain considerable error. Nor can it be due to the failure of the condensation calculation to consider Ti–Al-rich pyroxene. No matter what the composition of the clinopyroxene, it is a relatively late phase in the condensation sequence (GROSSMAN and CLARK, 1973), appearing well below the temperatures at which both Ca and Al are totally condensed, ~1550°K at 10^{-3} atm. Condensation of later phases, including pyroxene, should dilute these elements but the Ca/Al ratio should remain constant. Type A inclusions appear to have a near-cosmic Ca/Al ratio but the Type B inclusions seem depleted in Ca relative to Al. This would indicate that the Type B's are not the descendants of Type A's which continued to react with the vapor to slightly lower temperatures but may themselves be disequilibrium condensates (WALTER and DODD, 1973). Alternatively, they may have had a more complex history than the Type A's, involving post-condensation differentiation. With regard to this problem, it would be interesting to compare the measured bulk chemical compositions of a large number of both

types of inclusions with variation diagrams predicted by condensation calculations. Note that the condensation temperatures inferred here on the basis of bulk chemical composition hold even if the inclusions were melted after condensation, as long as melting and recrystallization were isochemical.

Condensate textures

As suggested by GROSSMAN (1972), the textural relations in the Ca-rich inclusions described by FUCHS (1969) and KURAT (1970) can be explained in terms of the calculated sequence of condensation reactions. These inclusions contain perovskite crystals embedded in an intimate intergrowth of spinel with a melilite having variable, but low, åkermanite content (<Ak35). Surrounding these aggregates and cavities in their interiors are narrow rims of diopside. The low FeO concentration (<1 per cent) in this diopside indicates that the mineral is not a reaction product between the edges of the aggregates and the FeO-rich matrix. Rather, the diopside rims are interpreted to be the product of the condensation reaction of melilite with the vapor. Several of the Type A inclusions described in this paper are similar in texture to those reported by Fuchs and by Kurat and thus could be high-temperature condensate aggregates preserved in their original solid form.

There are only two other textural features in the inclusions which argue strongly for condensation from a vapor phase. Acicular wollastonite crystals projecting into cavities were observed on slab surfaces in one Type A and one Type B inclusion. These have also been noted by FUCHS (1971, 1974). Such textures are characteristic of vapor-deposited phases in laboratory syntheses and in natural vugs and geodes. Wollastonite does not appear in the equilibrium condensation sequence but could form during slight departures from equilibrium because the nebula is only slightly undersaturated with respect to it at 1450°K. The rare, sinuous Type A inclusions possess very delicate arborescent structures which could have grown while suspended in a vapor. Their shapes make it difficult to imagine that they are solidified liquids.

Evidence of melting

Many of the textural characteristics of both types of inclusions could be interpreted in terms of crystallization from a liquid. These include the coarse interlocking crystals of pyroxene and melilite (Figs. 1B and 1D), the laths of anorthite and melilite (Fig. 1D) and the poikilitic spinels (Fig. 2A). SEITZ and KUSHIRO (1974) melted a Type B inclusion and studied its liquid–crystal phase relations. At atmospheric pressure, spinel is the first phase to crystallize, followed by clinopyroxene, plagioclase and, finally, melilite. This crystallization sequence is consistent with many of the textural observations made in this study, such as the poikilitic spinels and the melilite which replaces pyroxene and plagioclase.

The perovskite grains are often particularly suggestive of a liquid origin. They commonly occur as long trails of spherical blebs (Fig. 2C) which could be solidified liquid droplets. Sometimes, they are present as vermicular intergrowths with melilite (Fig. 2D) which could be interpreted in terms of eutectic crystallization, devitrification of a glass or secondary replacement. FUCHS (1974) argued that the presence of grossularite in some inclusions requires a liquid origin because it is

unstable relative to other phases at the proposed condensation temperatures of the inclusions. The relatively rare grossularite, however, could have formed during disequilibrium condensation for the same reason as wollastonite and might have persisted as a metastable condensate. None of the above indicators point unambiguously to a liquid origin.

There are, however, some stronger suggestions for the existence of liquid. The presence of rare nickel–iron grains inside perovskite crystals cannot be explained by the condensation model. Perovskite should have condensed almost 200°K higher than the metal. Furthermore, even if these phases condensed together, the great abundance of Fe relative to Ca and Al and the steep condensation curve of Fe would have resulted in inclusions dominated by metallic iron with relatively minor amounts of Ca–Al-rich phases. Also, even FeO concentrations as low as those in the pyroxenes and spinels are not expected for high-temperature solar nebula condensates. FeO contents on the order of 1 per cent can only occur when the nebula becomes more oxidizing at temperatures below ~800°K. It could be argued that such inclusions underwent a mild metasomatism in which the pyroxenes and spinels incorporated FeO which diffused into the inclusions from the matrix. Many of the crystals involved, however, look relatively fresh and unaltered. An alternative possibility is that the early condensates were mixed with very small amounts of lower-condensing materials (e.g. nickel–iron, Fe-bearing silicates, etc.) and that these composite aggregates were melted and then frozen in the nebula.

GROSSMAN and CLARK (1973) showed that certain critical phase assemblages should be present in the inclusions if they condensed in the P–T stability field of partial melts. From published descriptions of only a few inclusions, they were able to rule out the condensation of partial melts based partly on the rarity of the assemblage gehlenite–hibonite–anorthite which would have crystallized from melts condensing along the corundum–gehlenite join. This assemblage was never found in this study. Hibonite was observed in only one Type A inclusion. Anorthite is very rare in the Type A's. If these inclusions were once melted, this occurred after condensation. This, in turn, places an upper limit of $\sim 2{\cdot}2 \times 10^{-3}$ atm to the pressure in that part of the nebula where the inclusions formed (GROSSMAN and CLARK, 1973). Alternatively, they might have condensed as supercooled liquids (FUCHS, 1974), but there is little strong evidence for this.

In spite of the suggestions that the inclusions were once molten, there is some very strong oxygen isotope evidence to the contrary. CLAYTON *et al.* (1974) found very large oxygen isotopic differences between different density fractions of a single, 'igneous-looking' Type B inclusion, TS23 F1 (Fig. 1D). These anomalies are not due to chemical isotope effects but may have been produced when small amounts of pre-existing, refractory interstellar grains with a unique isotopic composition were incorporated by the condensate minerals (CLAYTON *et al.*, 1973). Regardless of their origin, the isotopic heterogeneities preserved within the inclusion indicate that it was never molten.

The clinopyroxene

GROSSMAN and CLARK (1973) considered the presence of clinopyroxenes with high TiO_2 contents as evidence that the inclusions did not crystallize from a

Table 10. Inclusions in this study whose oxygen isotopic compositions were measured by CLAYTON *et al.* (1973)

Inclusion	Type	Sample Number (Clayton *et al.*)	δO^{18} (SMOW)
TS2 F1	A	A1 7	+0·7
TS4 F1	B	A1 13	−12·4
TS8 F3	B	A1 14	−14·8
TS23 F1	B	A1 15	−17·0
TS24 F1	A	A1 6	+0·6

liquid. This was based partly on work by YAGI and ONUMA (1967) who found that a maximum of only 11 per cent $CaTiAl_2O_6$ (~4 wt. % TiO_2) can dissolve in diopside and partly on the fact that metastable pyroxenes equilibrate their compositions rapidly when in contact with a silicate melt. When SEITZ and KUSHIRO (1974) melted a Type B inclusion, they produced a pyroxene containing 4·3 per cent TiO_2 at 1250°C and 7 kbar pressure. There is no indication of how they determined the oxidation state of the Ti. There is now considerable evidence that a large fraction of the Ti in the Allende pyroxenes is trivalent and it may be that the data of YAGI and ONUMA (1967) are not applicable to them. By crudely estimating the free energy of $CaTiAl_2O_6$, GROSSMAN and CLARK (1973) suggested that pyroxenes containing large amounts of this molecule might have condensed from the nebula. It is also likely that trivalent Ti could have dissolved in this mineral since Ti_3O_5 is a stable condensate at 1393°K at 10^{-3} atm (GROSSMAN, 1972). At the present state of knowledge, however, the presence of this pyroxene cannot be used as a strong argument for or against molten inclusions.

Shock and fragmentation

The deformation lamellae (Fig. 1C) and undulose extinction of the pyroxene and melilite in some inclusions suggest a shock event in their history. In some cases, this may have caused partial melting and recrystallization into polycrystalline mosaics of melilite. One of these mosaics contains interstitial, ragged, elongated grains of spinel (Fig. 2B). In addition, there is abundant evidence that both types of inclusions were broken at a very early date. Many of the inclusions studied are brecciated. In these cases, fragments of the same inclusion are adjacent to one another with a small amount of intervening matrix. This indicates breakage and slight relative motion after incorporation into the parent body. Very often, however, only small, single, angular fragments are seen both in thin section and in three dimensions in the slabs. This suggests that these inclusions were broken prior to or during their incorporation. This may have occurred during collisions between aggregates in the nebula. The fact that a larger fraction of the Type A's appears to be broken and that the mean size of the Type A fragments is less than that of the Type B fragments indicates that the collision frequency, and therefore probably also the dust concentration, was higher in the region of the nebula where the Type A's were stored.

Metamorphism

Not a single grain of nepheline or sodalite was found in this study of 26 randomly-selected, coarse-grained, Ca-rich inclusions. Non-zero count rates for

Na and Cl were sometimes observed in the opaque, fine-grained interstitial material and, more often, in the opaque zones found inside the inclusions near their contacts with the matrix. Texturally, these elements must be regarded as secondary in origin, post-dating the primary crystals in the interiors of the inclusions. Whether they entered the inclusions while they were still suspended in the nebula (ARRHENIUS and ALFVÉN, 1971) or whether they are the result of exchange reactions between the matrix and inclusions after the accretion of the parent body (GROSSMAN, 1972) is still an open question. The data of GRAY *et al.* (1973) suggest that at least some of the alkalies may have entered the inclusions in the past 3·6 b.y., long after condensation was over. The relatively FeO-rich olivine overgrowths are sometimes found on the edges of brecciated inclusions, suggesting that the olivine post-dates accretion.

CONCLUSION

A complex record of condensation, fragmentation, accretion and metamorphism is preserved in the coarse-grained, Ca-rich inclusions in Allende. Which of these objects, if any, were melted and where they were metamorphosed are still unanswered questions. The exact relationships between the two varieties and between them and the fine-grained aggregates are likewise unknown. Collectively, these objects constitute less than 10 per cent of the meteorite. It is obvious that a vast amount of information about events in the early solar system can be revealed by detailed investigations of the whole range of different petrographic units in this meteorite and we are fortunate in having such a large amount of it available for study.

Acknowledgements—The author is indebted to Dr. E. OLSEN of the Field Museum of Natural History for making large quantities of the Allende meteorite available for this study. I. M. STEELE, T. SOLBERG, M. POINT and O. DRAUGHN gave valuable advice and assistance in the preparation of polished thin sections, operation of the electron microprobe and data reduction. Stimulating discussions with R. N. CLAYTON and T. K. MAYEDA are gratefully acknowledged. This work was supported by the Research Corporation, the National Aeronautics and Space Administration through grant NGR 14-001-249 and the Louis Block Fund of the University of Chicago.

REFERENCES

ANDERSON D. L. (1973) The composition and origin of the moon. *Earth Planet. Sci. Lett.* **18**, 301–316.

ARRHENIUS G. and ALFVÉN H. (1971) Fractionation and condensation in space. *Earth Planet. Sci. Lett.* **10**, 253–267.

CHRISTOPHE M. (1968) Un chondre exceptionnel dans la météorite de Vigarano. *Bull. Soc. Fr. Minéral. Cristallogr.* **91**, 212–214.

CHRISTOPHE M. (1969) Etude minéralogique de la chondrite CIII de Lancé. In *Meteorite Research*, (editor P. M. Millman), pp. 492–499. Reidel.

CLARK S. P., JR., TUREKIAN K. K. and GROSSMAN L. (1972) Model for the early history of the earth. In *The Nature of the Solid Earth*, (editor E. C. Robertson), pp. 3–18. McGraw-Hill.

CLARKE R. S., JR., JAROSEWICH E., MASON B., NELEN H., GÓMEZ M. and HYDE J. R. (1970) The Allende, Mexico, meteorite shower. *Smithson. Contrib. Earth Sci.* **5**.

CLAYTON R. N., GROSSMAN L. and MAYEDA T. K. (1973) A component of primitive nuclear composition in carbonaceous meteorites. *Science* **182**, 485–488.

CLAYTON R. N., GROSSMAN L., MAYEDA T. K. and ONUMA N. (1974) Heterogeneities in the solar nebula. Paper to appear in the *Proceedings of the Soviet–American Conference on the Cosmochemistry of the Moon and the Planets*, Moscow.

DOWTY E. and CLARK J. R. (1973) Crystal structure refinement and optical properties of a Ti^{3+} fassaite from the Allende meteorite. *Amer. Mineral.* **58,** 230–242.

FROST M. J. and SYMES R. F. (1970) A zoned perovskite-bearing chondrule from the Lancé meteorite. *Mineral. Mag.* **37,** 724–726.

FUCHS L. H. (1969) Occurrence of cordierite and aluminous orthoenstatite in the Allende meteorite. *Amer. Mineral.* **54,** 1645–1653.

FUCHS L. H. (1971) Occurrence of wollastonite, rhönite, and andradite in the Allende meteorite. *Amer. Mineral.* **46,** 2053–2067.

FUCHS L. H. (1974) Grossular in the Allende (type III carbonaceous) meteorite. *Meteoritics* **9,** 11–18.

GRAY C. M., PAPANASTASSIOU D. A. and WASSERBURG G. J. (1973) The identification of early condensates from the solar nebula. *Icarus* **20,** 213–239.

GROSSMAN L. (1972) Condensation in the primitive solar nebula. *Geochim. Cosmochim. Acta* **36,** 597–619.

GROSSMAN L. (1973) Refractory trace elements in Ca–Al-rich inclusions in the Allende meteorite. *Geochim. Cosmochim. Acta* **37,** 1119–1140.

GROSSMAN L. (1974) Chemical fractionation in the solar nebula. Paper to appear in the *Proceedings of the Soviet–American Conference on the Cosmochemistry of the Moon and the Planets*, Moscow.

GROSSMAN L. and CLARK S. P., JR. (1973) High-temperature condensates in chondrites and the environment in which they formed. *Geochim. Cosmochim. Acta* **37,** 635–649.

HADIDIACOS C. G., FINGER L. W. and BOYD F. R. (1971) Computer reduction of electron probe data. *Carnegie Inst. Wash. Yearb.* **69,** 294.

KEIL K. and FUCHS L. H. (1971) Hibonite [$Ca_2(Al, Ti)_{24}O_{38}$] from the Leoville and Allende chondritic meteorites. *Earth Planet. Sci. Lett.* **12,** 184–190.

KRÄHENBÜHL U., GANAPATHY R., MORGAN J. W. and ANDERS E. (1973) Volatile elements in Apollo 16 samples: implications for highland volcanism and accretion history of the moon. *Proc. Fourth Lunar Sci. Conf., Geochim. Cosmochim. Acta Suppl.* **4,** Vol. 2, pp. 1325–1348. Pergamon Press.

KURAT G. (1970) Zur Genese der Ca–Al-reichen Einschlüsse im Chondriten von Lancé. *Earth Planet. Sci. Lett.* **9,** 225–231.

LARIMER J. W. and ANDERS E. (1970) Chemical fractionations in meteorites—III. Major element fractionations in chondrites. *Geochim. Cosmochim. Acta* **34,** 367–387.

MALISSA H., JR., HERMANN F., KLUGER F. and KIESL W. (1972) Chemical and microprobe investigations of the Allende meteorite. *Mikrochim. Acta* **3,** 434–450.

MARVIN U. B., WOOD J. A. and DICKEY J. S., JR. (1970) Ca–Al-rich phases in the Allende meteorite. *Earth Planet. Sci. Lett.* **7,** 346–350.

REID A. M., WILLIAMS R. J., GIBSON E. K., JR. and FREDRIKSSON K. (1974) A refractory glass chondrule in the Vigarano chondrite. *Meteoritics* **9,** 35–45.

SEITZ M. G. and KUSHIRO, I. (1974) Melting relations of the Allende meteorite. *Science* **183,** 954–957.

WALTER L. S. and DODD R. T., JR. (1973) Chemical variations among chondrules and aggregates in the Allende (C-3) meteorite. Preprint.

WÄNKE H., BADDENHAUSEN H., DREIBUS G., JAGOUTZ E., KRUSE H., PALME H., SPETTEL B. and TESCHKE F. (1973) Multielement analyses of Apollo 15, 16 and 17 samples and the bulk composition of the moon. *Proc. Fourth Lunar Sci. Conf., Geochim. Cosmochim. Acta Suppl.* **4,** Vol. 2, pp. 1461–1481. Pergamon Press.

YAGI K. and ONUMA K. (1967) The join $CaMgSi_2O_6$–$CaTiAl_2O_6$ and its bearing on the titanaugites. *J. Fac. Sci. Hokkaido Univ. Ser.* IV, **13,** 463–483.

APPENDIX

CLAYTON *et al.* (1973) discovered remarkable oxygen isotopic compositions in samples of anhydrous minerals removed from carbonaceous chondrites. They suggested that these phases contain oxygen having 'normal' isotopic composition mixed with a small amount of pure, or nearly pure, O^{16}. One possible explanation is that the O^{16} entered the solar nebula in the form of interstellar grains which escaped vaporization and homogenization during the early hot stage of the nebula and that they were incorporated by the high-temperature minerals as they condensed from the vapor with 'normal' solar system isotopic compositions. Several of the Allende samples whose isotopic compositions were reported by CLAYTON *et al.* (1973) are coarse-grained Ca-rich inclusions whose thin sections were analyzed in this study. Table 10 shows the correspondence between the sample numbers used by Clayton *et al.* and those employed here. It appears from the table that the Type B inclusions contain a higher concentration of the exotic component than the Type A's, suggesting that it may be associated in some way with the titaniferous pyroxene. This was also indicated by isotopic data on mineral separates from TS23 F1 (CLAYTON *et al.* 1974).